Lithium-ion Battery State of Charge Estimation Model Based on Kalman Filtering Algorithm and Equivalent Circuit

Xiao-Tian Wang, Ze-Zheng Zhang, Jie-Sheng Wang*, Song-Bo Zhang, Xun Liu

Abstract—**In recent years, electric vehicles have garnered significant attention, with lithium-ion batteries (LIBs) being central to their operation. Researchers and scholars have prioritized the accurate estimation of the state of charge (SOC) within the battery management system (BMS) as a key area of study. In this paper, by analyzing different equivalent circuit models, we choose to use the second-order RC model, elaborate the Kalman filter (KF) principle, and propose the adaptive extended Kalman filter (AEKF) to construct the estimation model of SOC. MATLAB validates the AEKF estimation model under two different operating conditions, UDDS and LA92, and the results show that the designed model can efficiently and accurately estimate the battery charge state with high competitiveness and accurately predict the real SOC direction regardless of the initial state, AEKF is more competitive than KF in terms of SOC prediction accuracy, Despite the different initial values of SOC, the root-mean-square error of prediction was able to be controlled around one percent.**

Index Terms—**soc estimation, extended Kalman filter, adaptive extended Kalman filter, equivalent circuit modeling**

I. Introduction

Battery SOC prediction has received widespread attention as a critical technology in EVs and renewable energy systems. Nowadays, EVs and all kinds of new electrical industries use batteries as a critical necessity, the research for battery SOC prediction involves a variety of fields, such as electrochemical modeling, statistical learning methods, deep learning algorithms and various methods are constantly evolving and improving. However, battery SOC prediction faces challenges in many aspects, including changes in battery characteristics, environmental impacts, data uncertainty, and so on. Therefore, improving the accuracy and stability of battery SOC prediction is essential [1-4].

For LIBs, SOC prediction is broadly categorized into three methods, which are based on electrochemical, physical, and deep learning models. For electrochemical models, Clemente et al. proposed an observer-based method that allows a real-time estimation of the SOC of vanadium redox flow batteries [5]. Wang et al. proposed an impedance spectrum-based detection method to predict the SOC of LIBs [6]. They demonstrated that although battery aging affects the internal resistance fluctuation of the battery, there is no effect on the charge transfer. Huang et al. proposed an interactive multi-country model (IMM) for estimating the SOC of LIBs based on electrochemical impedance spectroscopy and used Untraceable Kalman Filtering (UKF) better to solve the nonlinear problem in SOC [7]. Predicting the SOC of LIBs based on physical models has gained the attention of many researchers due to the existence of factors such as complexity and uncertainty in electrochemical models. Gao et al. proposed a physically based enhancement for predicting the SOC of LIBs while separating the voltage hysteresis phenomenon from the battery voltage and modeling it using a single-state hysteresis formulation [8]. The other contributions to the voltage are made through the calculation of physical models, and a discrete-time implementation algorithm simplifies the extended model to achieve accurate prediction of the SOC of LIBs. Chen et al. proposed a lithium-ion battery charge state estimation based on fractional order modeling and adaptive square root volume Kalman filtering [9]. Gu et al. proposed the modified multi-innovation adaptive EKF algorithm for identifying battery SOC algorithm of LIBs with the addition of an attenuation factor to the weighted fusion of innovation vectors for present/past innovations [10].

To save computational cost and simplify the SOC prediction step, many researchers carry out studies in the direction of deep learning, where historical data, such as voltage and current, serve as inputs for deep learning algorithms, and historical SOC data are used as prediction targets to achieve the purpose of predicting the SOC through a kind of nonlinear mapping. Wang et al. proposed a closed-loop framework based on a deep convolutional neural network (DCNN) [11]. The data features were extracted using the convolutional and pooling layers of the convolutional neural network, and the network was optimized using migration learning and pruning operations. Huang et al. proposed a feed-forward neural network (FNN)

Manuscript received January 17, 2024; revised April 16, 2024. This work was supported by the Basic Scientific Research Project of Institution of Higher Learning of Liaoning Province (Grant No. LJKZ0293), and Postgraduate Education Reform Project of Liaoning Province (Grant No. LNYJG2022137).

Xiao-Tian Wang is a postgraduate student of School of Electronic and Information Engineering, University of Science and Technology Liaoning, Anshan, 114051, P. R. China (e-mail: 2207942300@qq.com).

Ze-Zheng Zhang is a postgraduate student of School of Electronic and Information Engineering, University of Science and Technology Liaoning, Anshan, 114051, P. R. China (e-mail: 1449446839@qq.com).

Jie-Sheng Wang is a professor of School of Electronic and Information Engineering, University of Science and Technology Liaoning, Anshan, 114051, P. R. China (Corresponding author, phone: 86-0412-2538246; fax: 86-0412-2538244; e-mail: wang_jiesheng@126.com).

Song-Bo Zhang is a postgraduate student of School of Electronic and Information Engineering, University of Science and Technology Liaoning, Anshan, 114051, P. R. China (e-mail: 2092926911@qq.com).

Xun Liu is a postgraduate student of School of Electronic and Information Engineering, University of Science and Technology Liaoning, Anshan, 114051, P. R. China (e-mail: heidengxiaguo@163.com).

complex based on the analysis of ultrasonic transmission signals from LIBs for accurate charge state prediction [12]. During the same year, Zhao et al. proposed a SOC prediction study based on the fusion of attention mechanism (AM) with convolutional neural network and gated neural unit (GRU) deep learning [13]. Since the LIBs SOC is closely related to time, Huang [14] proposed a deep learning time series prediction based problem. Chen et al. proposed an LSTM-RNN with extended inputs and restricted outputs for SOC estimation of LIBs [15].

The work in this paper is to develop a battery SOC estimation model through the comparison of various estimation methods, and finally, the SOC is estimated by modeling the SOC using the AEKF method and the SORC equivalent circuit and verified by simulation using MATLAB. The structure is delineated as follows. Part I: Introduction, mainly describes the research background and practical significance of the topic of battery SOC estimation model based on KF algorithm and equivalent circuit. The current research status of battery SOC estimation and future development are introduced in detail. Part II: Introduces the KF algorithm and equivalent circuit, analyzes the advantages and disadvantages of different identical circuit models, proposes the circuit model selected in this paper, explores the principle of KF, and further introduces the methods of EKF and AEKF. Part III: Simulation experiments and results analysis: this paper mainly selects the Turnigy Graphene 5000mAh 65C LIBs data for simulation verification. Under the two different working conditions of UDDS and LA92, the validity of the battery SOC estimation of the AEKF algorithm is verified, compared, and analyzed with the EKF algorithm, and the original value of the SOC estimation is changed to check the convergence performance of the AEKF algorithm.

II. Kalman Filtering Algorithms and Equivalent Circuits

This subsection provides a more detailed description of standard equivalent circuit models and gives the second-order RC model used; it introduces the basic theory of KF, with an emphasis on the extended Kalman filter and AEKF. This paper aims to establish a battery SOC estimation model through comparison of various estimation methods. The SOC is then estimated using the adaptive extended Kalman filter method and the SORC equivalent circuit model. Finally, the model's accuracy is verified through simulation using MATLAB.

A. Introduction to Battery Equivalent Circuit Modeling

(1) Rint Model

As depicted in Fig. 1 and Eq. (1), the open circuit voltage of the battery is defined by an ideal voltage source U_{oc}. The voltage source U_{oc} is an ohmic resistance. R_0 denotes the ohmic resistance. I_L signifies the load current, and U_L represents the terminal voltage.

$$U_L = U_{oc} - I_L R_o \tag{1}$$

Since the Rint model does not consider the changing characteristics within the battery and the difference in electrolyte concentration, the Rint model is only valid for steady-state load conditions because it responds too quickly to the changing voltage of the load; the limitations are twofold, firstly, the Rint model reacts too quickly to the changing voltage of the load, secondly, the internal resistance does not vary with the magnitude of the current [16].

(2) RC Model

The RC model depicted in Fig. 2 comprises three resistors denoted as R_1, R_2, and R_3, along with two capacitors labeled as C_1 and C_2. Capacitor C_1 is a surface capacitance. Capacitor C_2 is a large capacitance, and a large capacitance represents sufficient capacity of the battery. C_2 has a significant weight on the estimation because it represents most of the energy in the battery. R_1 and R_2 are the termination resistors, and R_3 is the capacitance resistor. U_1 and U_2 are the voltages of the C_1 and C_2 capacitors. Eq. (2) and Eq. (3) represent the electrical characteristics of the RC circuit.

$$\begin{bmatrix} U_1 \\ U_2 \end{bmatrix} = \begin{bmatrix} \dfrac{-1}{C_1(R_1+R_3)} & \dfrac{1}{C_1(R_1+R_3)} \\ \dfrac{1}{C_2(R_1+R_3)} & \dfrac{-1}{C_2(R_1+R_3)} \end{bmatrix} \begin{bmatrix} U_1 \\ U_2 \end{bmatrix} + \begin{bmatrix} \dfrac{-R_3}{C_1(R_1+R_3)} \\ \dfrac{-R_1}{C_2(R_1+R_3)} \end{bmatrix} [I] \tag{2}$$

$$[U_L] = \begin{bmatrix} \dfrac{R_3}{(R_1+R_3)} & \dfrac{R_1}{(R_1+R_3)} \end{bmatrix} \begin{bmatrix} U_1 \\ U_2 \end{bmatrix} + \begin{bmatrix} \dfrac{R_1 R_2}{(R_1+R_3)} \end{bmatrix} [I] \tag{3}$$

(3) Thevenin Model

The Thevenin model considers the similar characteristics of batteries and capacitors and adds an RC link, C_1 represents the polarization capacitance while R_1 denotes the polarization resistance. The abrupt resistance characteristics in the model are simulated by R_0, and the voltage gradient capacitance characteristics are affected by R_1 and C_1. Fig. 3 illustrates the schematic diagram of the Thevenin model, which comprises three components: open circuit voltage U_{oc}, internal resistance R_0, and capacitance C_1. The internal resistance is denoted as R_0, while the capacitance is represented by C_1. U_L represents the terminal voltage, and I_L denotes the current. Equations (4) and (5) define the electrical characteristics of the Thevenin model circuit.

$$U_1 = -\frac{U_1}{R_1 C_1} + \frac{I_L}{C_1} \tag{4}$$

$$U_L = U_{oc} - U_1 - I_L R_o \tag{5}$$

(4) PNVG Model

The PNGV model offers ease of implementation and provides a more precise depiction of the battery's dynamic characteristics. The model structure, as illustrated in Fig. 4, includes key parameters such as open circuit voltage U_{ocv}, battery capacitance C_b, internal resistance of the battery R_e, battery polarization resistance R_p, battery polarization capacitance C_p, terminal voltage of the battery U_d, circuit current I, U_b represents the voltage capacitance at the two terminals of component C_b, while U_p denotes the voltage across the terminals of capacitance

C_p .The corresponding equations are detailed in Eq. (6)-(8):

$$U_d = U_{ovc}(SOC,T) - U_b - U_p - I \times R_e \tag{6}$$

$$\dot{U}_b = \frac{1}{C_b} \times I \tag{7}$$

$$\dot{U}_p = -\frac{1}{C_p \times R_p} \times U_p + \frac{1}{C_p} \times I \tag{8}$$

where $U_{ocv}(SOC,T)$ denotes the open circuit voltage at different SOC levels and temperatures, while $\dot{U}_b$ represents the differential operation of voltage U_b . Furthermore, $\dot{U}_p$ signifies the differential operation of voltage U_p . The equation is then discretized and can be expressed as:

$$U_d^t = U_{ocv}\left(SOC_t, T_t\right) - U_b^t - I_t \times R_e \tag{9}$$

$$U_b^t = U_b^{t-1} + \left(\frac{\Delta t}{C_b}\right) I_t \tag{10}$$

$$U_p^t = \exp\left(\frac{-\Delta t}{(C_p R_p)}\right) U_p^{t-1} + R_p\left(1 - \exp\left(\frac{-\Delta t}{(C_p R_p)}\right)\right) I_t \tag{11}$$

where U_d^t represents the terminal voltage at time *t*, $U_{ocv}(SOC_t, T_t)$ denotes the open-circuit voltage associated with SOC_t and the temperature value at time *t*. Furthermore, U_b^t and U_p^t are the terminal voltages of components C_b and C_p , respectively, at time *t* in the PNGV model. Additionally, Δt is a simple period, and I_t is the current measured by the power cell at time *t*.

(5) PNVG Model

The second-order RC model is derived from the Thevenin model, incorporating an RC network in series as depicted in Figure 5. This model comprises three key components: the open-circuit voltage V_{ocv} , internal resistance R_0 , and two RC networks. Specifically, R_1 represents the electrochemical polarization resistance, R_2 denotes the concentration polarization resistance, C_1 signifies the electrochemical polarization capacitance, and C_2 represents the concentration polarization capacitance. Additionally, V_t symbolizes the terminal voltage of the cell as described in Eq. (12) - (14).

$$V_1 = \frac{V_1}{R_1 C_1} + \frac{I}{C_1} \tag{12}$$

$$V_2 = -\frac{V_2}{R_2 C_2} + \frac{I}{C_2} \tag{13}$$

$$V_L = V_{oc} - V_1 - V_2 - IR_0 \tag{14}$$

B. Equivalent Circuit Model Used in This Paper

Using the second order RC model will improve the accuracy of the system, but it will make the battery model more complex, which is acceptable; According to the Ah integral method, the SOC is calculated as follows:

$$SOC_{k+1} = SOC_k - \frac{\eta \Delta t I_k}{C_n} \tag{15}$$

where, C_n denotes the cell capacity; η denotes the Coulombic efficiency. Eq. (12)-(13) are in discrete transformed form:

$$V_{1,k+1} = \exp\left(-\frac{\Delta t}{\tau_1}\right) V_{1,k} + R_1\left(1 - \exp\left(-\frac{\Delta t}{\tau_1}\right)\right) I_k \tag{16}$$

$$V_{2,k+1} = \exp\left(-\frac{\Delta t}{\tau_2}\right) V_{2,k} + R_2\left(1 - \exp\left(-\frac{\Delta t}{\tau_2}\right)\right) I_k \tag{17}$$

$$V_{t,k} = V_{oc,k} - V_{1,k} - V_{2,k} - I_k R_0 \tag{18}$$

In accordance with the second-order RC cell model, the state space equation can be formally expressed as shown in Eq. (19).

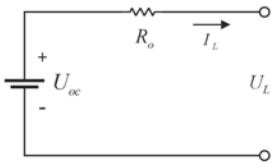

Fig. 1 Schematic diagram of the Rint model.

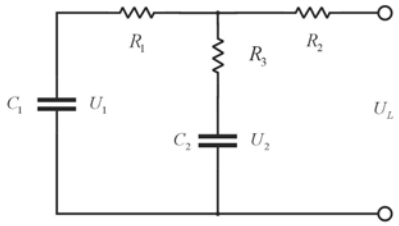

Fig. 2 Schematic diagram of RC model.

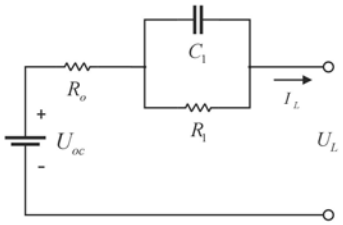

Fig. 3 Schematic diagram of Thevenin model.

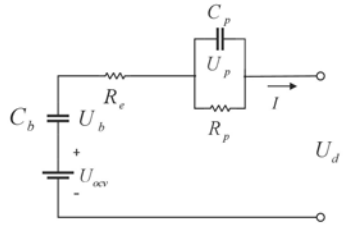

Fig. 4 Schematic diagram of the PNGV model.

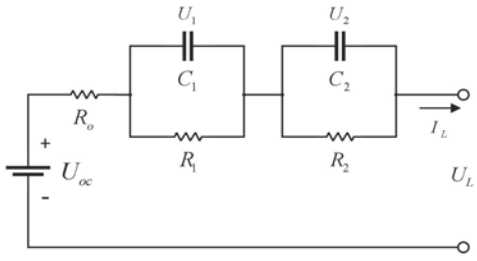

Fig. 5 Schematic diagram of the second-order RC model.

$$\begin{bmatrix} V_{1,k+1} \\ V_{2,k+1} \\ SOC_{k+1} \end{bmatrix} = \begin{bmatrix} \exp\left(\frac{-\Delta t}{\tau_1}\right) & 0 & 0 \\ 0 & \exp\left(\frac{-\Delta t}{\tau_2}\right) & 0 \\ 0 & 0 & 1 \end{bmatrix} \times \begin{bmatrix} V_{1,k} \\ V_{2,k} \\ SOC_k \end{bmatrix} + \begin{bmatrix} R_1 \times \left(1 - \exp\left(\frac{-\Delta t}{\tau_1}\right)\right) \\ R_2 \times \left(1 - \exp\left(\frac{-\Delta t}{\tau_2}\right)\right) \\ -\frac{\eta \Delta t}{C_n} \end{bmatrix} \times I_k + w \tag{19}$$

where, R_1, C_1, R_2, and C_2 are RC model parameters, Δt is the sampling time in seconds, w_k is the noise parameter, and V_1 is the voltage of R_1. V_2 is the voltage of R_2. The parameters τ_1 and τ_2 are the time constants of the RC network, which are equal to $\tau_1 = R_1 C_1$ and $\tau_2 = R_2 C_2$.

C. Principles of Kalman Filtering

The KF algorithm is a generalized algorithm for estimating system parameters. The KF can be thought of as a black box. The KF has an input and an output. The input is inaccurate measurements that are noisy. Outputs are more accurate, and estimates are less noisy. The estimates can be unmeasured or unobserved system state parameters. Similarly, the KF can estimate unobserved or unmeasured system parameters. KF algorithm linear discrete system equations of state and observed equations are:

$$x_k = Ax_{k-1} + Bu_k + w_k \tag{20}$$

where x_k denotes the value of the system state variable x at time point k, A represents the state transfer matrix from time point k-1 to the state variable x at time point k, B signifies the control input matrix for the control vector u_k, and w_k refers to the system noise vector with a covariance matrix Q_k that is conventionally distributed as $w_k \sim N(0, Q_k)$.

$$y_k = Cx_k + Du_k + v_k \tag{21}$$

where y_k denotes the value of the output variable of the system at time point k, and u_k represents the input to the system. Furthermore, C signifies the output matrix and D is the feed-forward matrix. v_k is the observation noise vector whose covariance matrix R_k is usually distributed, $v_k \sim N(0, R_k)$. KF is mainly divided into two processes: prediction and update. Based on the state and error covariance matrix at time point k, the prediction of the state and error covariance matrix at time point k+1 is computed as follows:

(22)

$$P_{k+1/k} = AP_kA^T + Q_k \tag{23}$$

$$K_k = P_{k+1/k}C^T\left(CP_{k+1/k}C^T + R_k\right)^{-1} \tag{24}$$

$$\hat{x}_{k+1} = \hat{x}_{k+1/k} + K_k\left(y_{k+1} - C\hat{x}_{k+1/k}\right) \tag{25}$$

$$P_{k+1} = \left(I - K_kC\right)P_{k+1/k} \tag{26}$$

D. Extended Kalman Filter Algorithm

The KF is suitable for linear systems, and nonlinear systems can be handled by the EKF. The EKF takes nonlinear systems by linearizing them and generating state estimates, this process is illustrated in Eq. (27)-(28).

$$x_{k+1} = f\left(x_k, u_k\right) + w_k \tag{27}$$

$$y_k = g\left(x_k, u_k\right) + v_k \tag{28}$$

where, w_k is the process noise of the system with covariance Q_k, $Q_k = E(w_k w_k^T)$, and v_k is the observation noise of the system with covariance R_k, $R_k = E(v_k v_k^T)$, both of which follow normal distribution and are independent, $w_k \sim N(0, Q_k)$, $v_k \sim N(0, R_k)$. $f(x_k, u_k)$ is the state transfer matrix function, and $g(x_k, u_k)$ is the measurement matrix function. Linear $f(x_k, u_k)$ and $g(x_k, u_k)$ to obtain:

$$f\left(x_k, u_k\right) \approx f\left(\hat{x}_k, u_k\right) = \frac{\partial f\left(x_k, u_k\right)}{\partial x_k}\Big|_{x_k = \hat{x}_k}\left(x_k - \hat{x}_k\right) \tag{29}$$

$$g\left(x_k, u_k\right) \approx g\left(\hat{x}_k, u_k\right) = \frac{\partial g\left(x_k, u_k\right)}{\partial x_k}\Big|_{x_k = \hat{x}_k}\left(x_k - \hat{x}_k\right) \tag{30}$$

Setting $A_k = \frac{\partial f\left(x_k, u_k\right)}{\partial x_k}\Big|_{x_k = \hat{x}_k}$, $C_k = \frac{\partial g\left(x_k, u_k\right)}{\partial x_k}\Big|_{x_k = \hat{x}_k}$, the linearized nonlinear system can be expressed as:

$$x_{k+1} \approx A_kx_k + \left[f\left(\hat{x}, u_k\right) - A_kx_k\right] + w_k \tag{31}$$

$$y_k \approx C_kx_k + \left[g\left(\hat{x}, u_k\right) - C_kx_k\right] + v_k \tag{32}$$

The steps of EKF are as follows:

$$\hat{x}_0 = E\left[x_0\right] \tag{33}$$

$$P_0 = E[(x_0 - \hat{x}_0)(x_0 - \hat{x}_0)^T] \tag{34}$$

$$\hat{x}_{k+1}^- = f\left(\hat{x}_k, u_k\right) \tag{35}$$

$$P_{k+1}^- = A_kP_kA_k^T + Q_k \tag{36}$$

$$K_{k+1} = P_{k+1}^-C_k^T(C_kP_{k+1}^-C_k^T + R_k)^{-1} \tag{37}$$

$$\hat{x}_{k+1} = \hat{x}_{k+1}^- + K_k[y_k - g(\hat{x}_{k+1}^-, u_k)] \tag{38}$$

$$P_{k+1} = (I - K_kC_k)P_{k+1}^- \tag{39}$$

The EKF algorithm is similar to the KF algorithm in that the optimal estimate of the state variable for the next moment is obtained by predicting the previous moment's estimate and then correcting it with the observed data.

E. Adaptive Extended Kalman Filter Algorithm

The AEKF algorithm, an advanced iteration of the EKF, addresses the challenge of covariance accuracy in state and observation equations that can impact estimation precision. It utilizes a covariance matching approach to dynamically adjust the R_k and Q_k covariance matrices as measurements evolve over time, thereby optimizing the prediction of state variables.

$$H_k = \frac{1}{N}\sum_{i=k-N+1}^{k} e_k e_k^T \tag{40}$$

$$Q_k = K_k H_k K_k^T \tag{41}$$

$$R_k = H_k - C_k P_k^- C_k^T \tag{42}$$

where, the new interest series e_k is the difference between the actual measured value and the predicted estimate, $e_k = y_k - \hat{y}_k$, according to the principle of open window estimation $e_k = y_k - \hat{y}_k$, H_k is the covariance function of e_k , N is the size of the open window, and K_k is the Kalman gain. The SORC model is employed, offering a clear and highly accurate physical interpretation that effectively describes the dynamic characteristics of the battery. The fundamental concept of KF involves utilizing both the output observation at the present moment and the state estimate from the previous moment to update the estimation of state variables. Additionally, by mitigating error and noise influence, the AEKF algorithm enhances estimation accuracy. A comprehensive grasp of these principles forms the basis for experimental simulation in Section III.

III. Simulation Experiments and Result Analysis

Through the introduction of the equivalent circuit and Kalman filter principle above. This chapter mainly focuses on the selection of data. It also introduces its analysis to verify the validity and feasibility of the model. The model is based on the AEKF algorithm under various working conditions and carries out the simulation using the KF method. The study conducts a comparative analysis of the strengths and weaknesses of the EKF algorithm in contrast to the AEKF algorithm model. Furthermore, it investigates the convergence behavior of the AEKF algorithm model under varying initial values of SOC. The paper also presents an analytical assessment to validate and demonstrate the feasibility of the proposed model.

A. Selection of Experimental Data

This paper was validated using data from Turnigy Graphene 5000mAh 65C Li-ion batteries, which were tested by Dr. Phillip Kollmeyer of McMaster University, Canada. The tests involved a new 5Ah Turnigy battery and were conducted at six different temperatures. Charging was performed at a rate of 1C to reach a voltage of 4.2V, with the battery temperature maintained at 25 degrees Celsius. Charging was terminated when the charge current reached 5mA. Additionally, four pulse-discharge HPPC tests (1C, 2C, 5C, and 10C discharge rates) were carried out along with corresponding charge tests (1C, 2C, 5C, and10 C).At 100, 95, 90, 80, 70..., 20, 15, 10, 5, and 2.5 % SOC) were performed at four different cycling conditions (UDDS, HWFET, LA92, and US06). Parameter identification from the test data yielded the parameter list of the SOC model in Table I, where the first column parameter is the SOC value from 0 to 1 representing different SOCs, the second column parameter is the ohmic resistor R0, the third column parameter is the electrochemical polarization resistor R1, the fourth column parameter is the concentration polarization resistor R2, the fifth column parameter is the electrochemical polarization resistor capacitance C1, and the sixth column parameter is the concentration polarization capacitance C2.

B. Experimental Results of AEKF Simulation for UDDS Conditions

In the simulation test conducted under the UDDS cycle condition, the initial SOC of the battery is set to 0.7, and the results are obtained through simulation. The results of the comparison between the AEKF voltage estimate and the measured value are shown in Fig. 6(a). The orange curve is the voltage estimate of the adaptive EKF algorithm, and the blue curve is the voltage measured value; the voltage estimate follows the calculated value closely, and the AEKF voltage estimate, and the measured voltage are in good agreement. The voltage comparison error is shown in Fig. 6(b) because the original value of SOC is set to 0.7, the voltage error is more significant at the beginning, the maximum error is calculated to be 274.3178mV, and the RMSE is 29.7100mV. In Figure 7(a), the orange curve represents the estimated battery SOC value obtained using the AEKF algorithm, while the blue curve depicts the battery SOC value derived from the Coulomb counting method. At the original stage of SOC estimation in the UDDS condition, there is a relatively large error between the estimated value of the AEKF algorithm and the Cullen counting value. The significant error is because the original value of the SOC is set to be 0.3 and the theoretical original value of the SOC is 1, but after that, the AEKF algorithm curve rapidly approaches the curve of Cullen's count value.

Table I. Parameter list of the second-order RC model

SOC	R0/mΩ	R1/mΩ	R2/mΩ	C1/F	C2/F
0	1.0001	0.4991	0.4956	20127	201696
0.1	12.8431	0.4979	0.4844	20529	207017
0.3	15.7735	0.4955	0.5034	20165	199004
0.3	10.5689	0.5064	0.4963	19555	202674
0.5	12.8425	0.5048	0.4970	19779	200848
0.6	10.1624	0.5046	0.4988	19592	202566
0.7	10.7265	0.4993	0.5011	20058	198330
0.8	10.1553	0.5057	0.4994	19775	200313
0.9	10.5078	0.4986	0.5004	19945	199863
1	10.4174	0.4977	0.5011	20219	201614

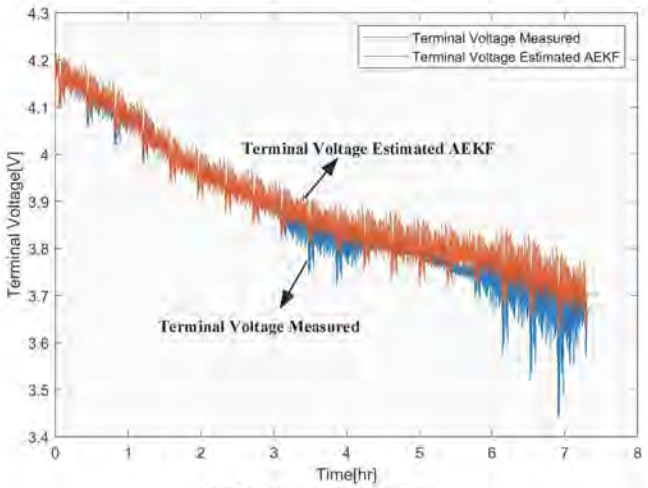

(a) Voltage contrast curves

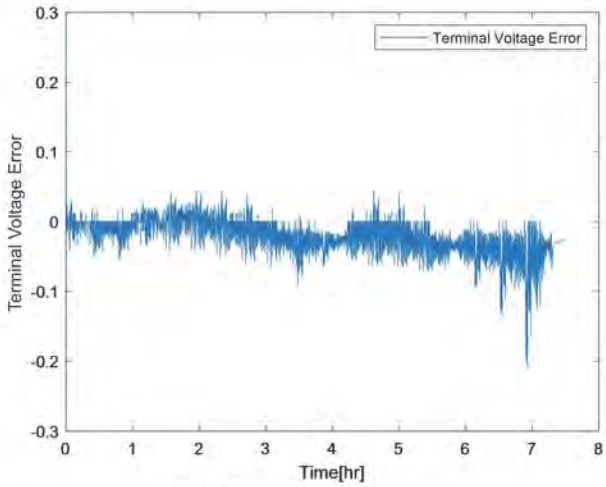

(b) Voltage contrast error curve

Fig. 6 Simulation comparison of estimated and measured AEKF voltage for UDDS condition.

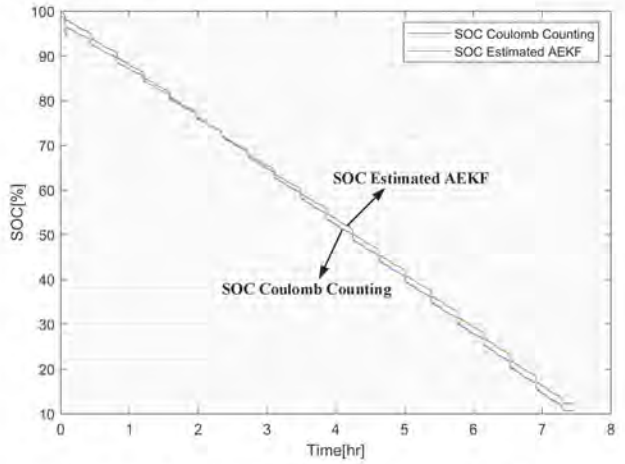

(a) Curve of cell SOC coulometric values vs. AEKF estimates

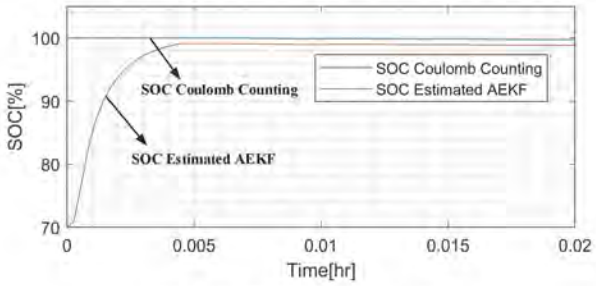

(b) Initial SOC comparison curve

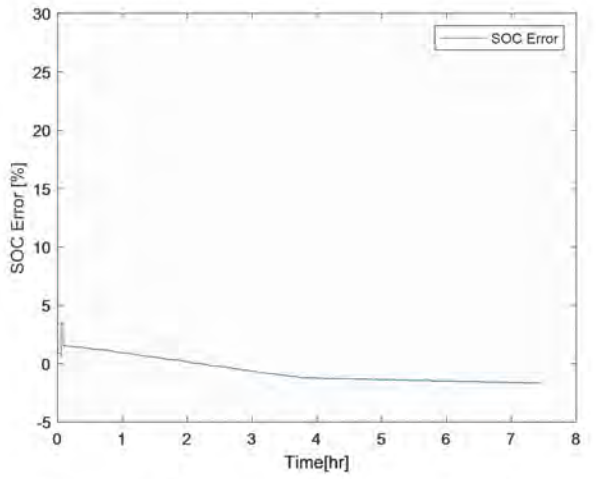

(c) Error curve of cell SOC coulometric values versus AEKF estimates

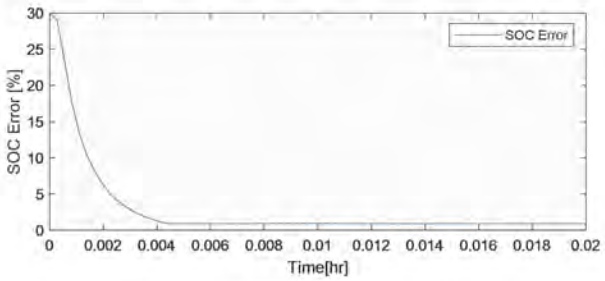

(d) Initial error curve

Fig. 7 AEKF simulation results for UDDS working conditions.

The discrepancy between the two values gradually diminishes. Upon computation, it is determined that the maximum SOC estimation error is 30%, with a root mean square error (RMSE) of 20.97%. This underscores the robust tracking capability of the AEKF algorithm.

C. Experimental Results of AEKF Simulation for LA92 Working Condition

LA92 (LA92 "Unified" Dynamometer Driving Schedule) is a light vehicle dynamometer driving schedule known as the Unified Cyclic Driving Schedule. Its duration is 1435 seconds, covering a total distance of 15.7 kilometers, with an average speed of 39.6 kilometers per hour. In the simulation under UDDS condition, the original value of SOC for both the battery and AEKF simulation is set to 0.7. The results are depicted in Figure 8.

Comparison results of AEKF voltage estimation and measurement under LA92 condition are shown in Fig. 9(a). The orange curve is the voltage estimation of the AEKF algorithm, and the blue curve is the voltage measurement; the voltage estimation follows the measurement closely, and AEKF voltage estimation matches the measured voltage better. The voltage comparison error is shown in Fig. 9(b) because the original value of SOC is set to 0.7, the voltage error is larger at the beginning, the maximum error is calculated to be 273.8188mV, and the RMSE is 27.5148mV.

D. Comparison of EKF and AEKF Simulation Results

Under LA92 conditions, two different algorithms, EKF and AEKF, are used to predict the SOC comparison test. The original conditions are the same SOC value. Figure 10(a) represents the SOC prediction curve of the two algorithms. The AEKF algorithm with the red line has a better prediction effect than the EKF algorithm with the green line, which is closer to the real SOC value, and the real time ability to track the change of SOC is also better than the EKF algorithm. It is also better than the EKF algorithm.

Fig. 10(b) illustrates the prediction results of the two algorithms at the initial stage of prediction. It is evident that the AEKF algorithm exhibits closer proximity to the actual value compared to the EKF algorithm. In general, both algorithms demonstrate improved capability in accurately estimating values within a short timeframe as depicted in Fig. (11). During the initial stage of SOC estimation, the AEKF-based algorithm outperforms its EKF-based counterpart, displaying not only faster convergence but also higher accuracy.

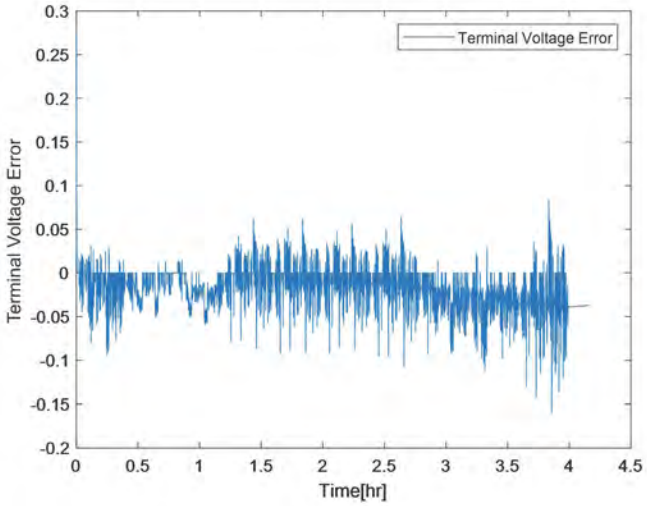

(a) Voltage contrast curves

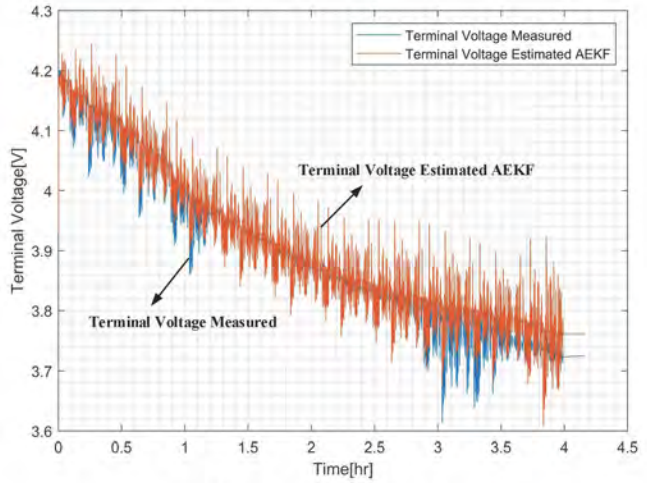

(b) Voltage contrast error curve

Fig. 8 Simulation comparison of predicted and measured AEKF voltage for LA92 condition.

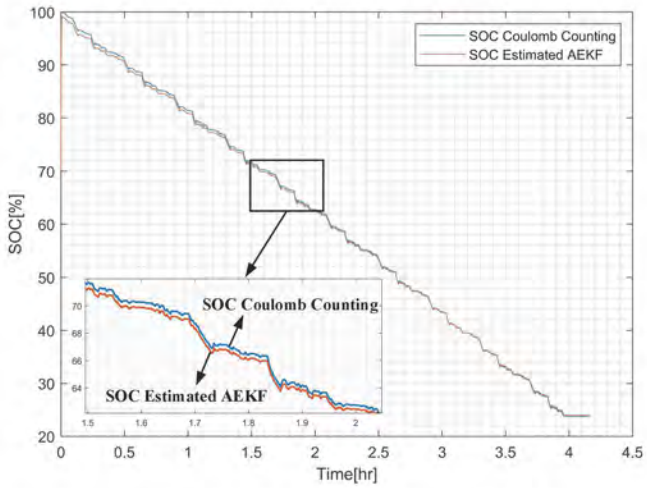

(a) Comparison curve of the theoretical value of battery SOC with the estimated value of AEKF

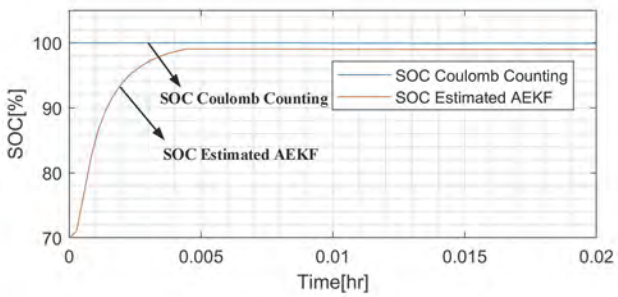

(b) Initial SOC comparison curve

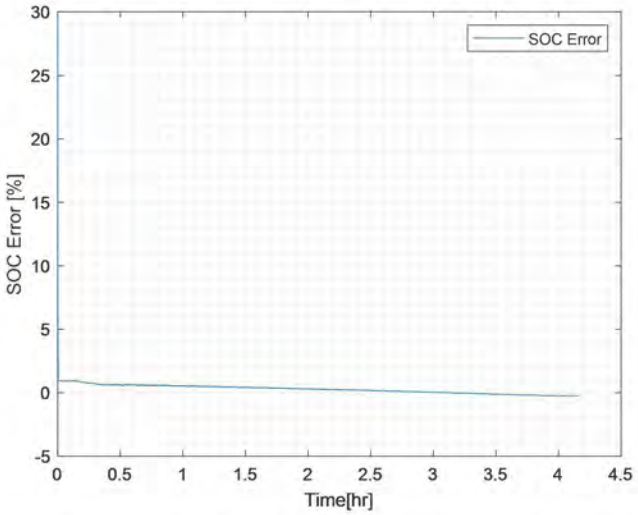

(c) Error curve of the theoretical value of cell SOC versus the AEKF estimate

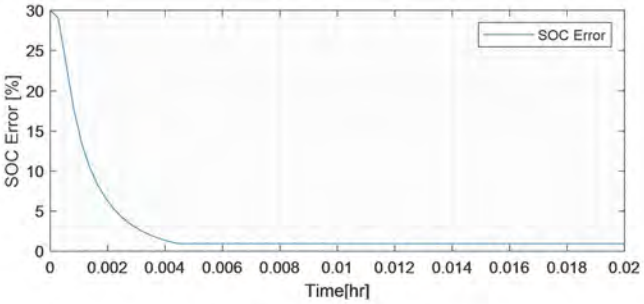

(d) Initial error curve

Fig. 9 AEKF simulation results for LA92 operating conditions.

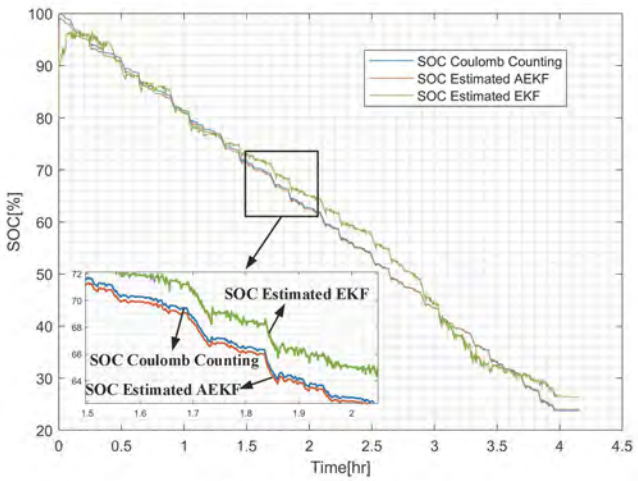

(a) SOC comparison curves

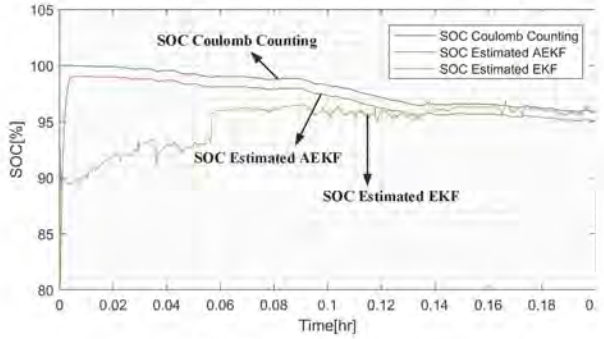

(b) Initial SOC comparison curve

Fig. 10 SOC estimation results for two different algorithms.

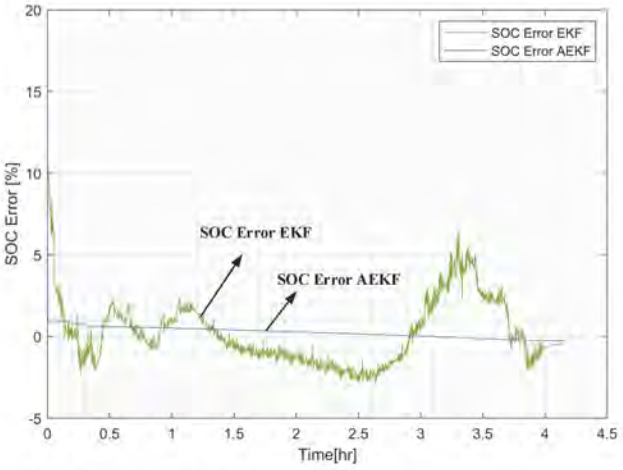

Fig. 11 SOC error curves for two different algorithms.

E. Validation of AEKF Algorithm for Original Value Convergence

By looking at the SOC estimation effect plots for the UDDS condition and the LA92 condition, we can see that the AEKF algorithm is able to quickly converge to a SOC value close to the Coulomb count value even if the initially set SOC value is not equal to the actual SOC value. An inaccurate estimation of the original SOC value will lead to error accumulation and may invalidate the filter. In practical production and applications, the accurate determination of the true original SOC value of the battery in different conditions poses a significant challenge, except when the battery is just filled or discharged when the SOC value can be directly obtained as 1 or 0. Therefore, it is essential to investigate the convergence effect of the AEKF algorithm under various initial values. To validate the convergence effect of the AEKF algorithm on the initial value, different original SOC values (0.5, 0.3, and 0.1) were set for testing under UDDS conditions The rest of the parameters were unchanged, and the simulation model was run to compare the estimation effects obtained under different original values. The comparison results were obtained as shown in Fig 12 - 14.

State 1: Set the original value of SOC estimated by the AEKF algorithm as 0.5.

As shown in Fig. 12, as the algorithm simulation operation continues to run, the SOC prediction value is constantly approaching the Coulomb count value and combining the SOC prediction value and the SOC Coulomb count value, the root-mean-square error is obtained as 1.3407% according to the root-mean-square error calculation formula.

State 2: Set the original value of SOC estimated by the AEKF algorithm as 0.3.

As shown in Fig. 13, as the algorithm simulation operation continues to run, the SOC prediction value is constantly approaching the Coulomb count value and combining the SOC prediction value and the SOC Coulomb count value, the RMSE is obtained as 1.4545% according to the root-mean-square error formula.

State 3: The original value of SOC estimated by the AEKF algorithm is set to be 0.1.

As depicted in Fig. 14, the orange curve represents the estimated battery SOC value obtained using the AEKF algorithm. Initially, there is a substantial discrepancy between the two curves; however, as the simulation progresses, the AEKF algorithm rapidly converges towards the Coulomb counting value. The distance between the two is getting smaller and smaller, and the RMSE is 1.5543% according to the formula of RMSE calculation. Error is 1.5543%.

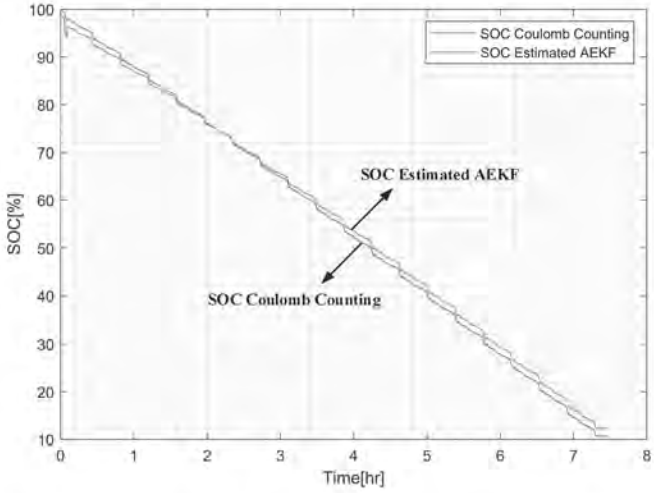

Fig. 12 Experimental results of SOC estimation simulation for initial value 0.5.

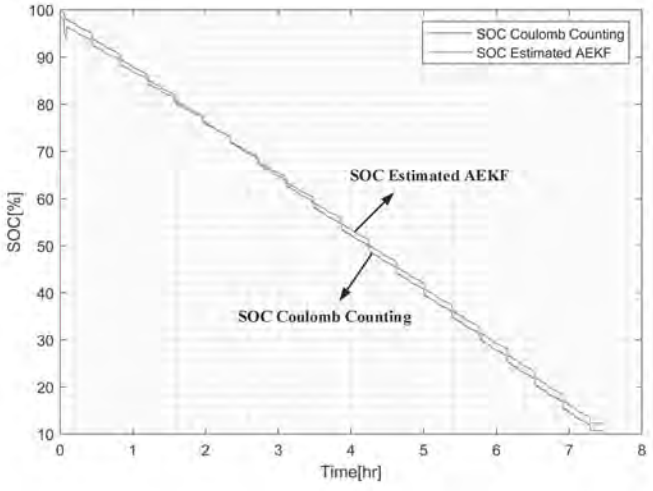

Fig. 13 Simulation experimental results of SOC estimation with initial value 0.3.

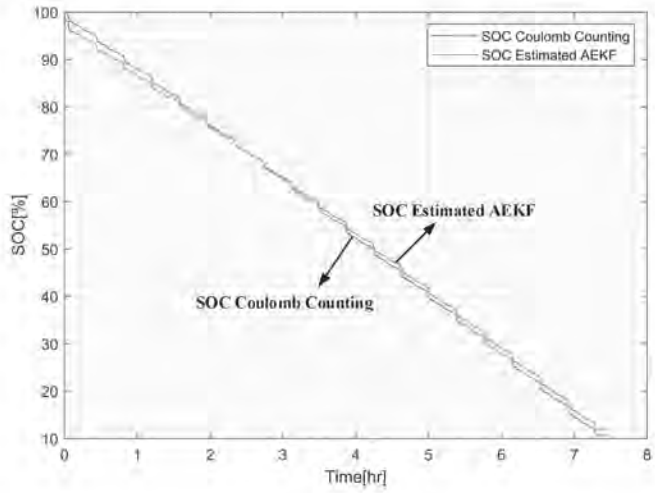

Fig. 14 Experimental results of SOC estimation simulation with initial value 0.1.

Through the analysis on the results of three groups experiments, when initial SOC values differ, the AEKF algorithm demonstrates strong convergence towards the erroneous original value. Employing the AEKF algorithm with various original SOC values facilitates rapid convergence towards the theoretical value. Shorter convergence times are observed, even with an initial value of 0.1. Gradual correction leads to approximation and close adherence to the theoretical value.

IV. Conclusion

This paper validates the effectiveness and accuracy of the battery SOC estimation model based on the AEKF algorithm under UDDS and LA92 operating conditions. The SOC estimation performance of the EKF and AEKF algorithms is compared through Matlab simulation experiments using data from Turnigy Graphene 5000mAh 65C LIBs. The results demonstrate that the AEKF algorithm exhibits faster convergence speed, better convergence accuracy, and robust convergence across different SOC original values. This SOC estimation approach holds significant implications for real-time monitoring and extending battery life in battery management systems. For practical application, an appropriate prediction model can be selected according to specific scenarios to enhance energy utilization efficiency, system stability of lithium-ion batteries, and mitigate security risks.

References

[1] C. W. Hua, J. S. Wang, and Y. Y. Chen. "Design and Performance Testing of Lead-acid Battery Experimental Platform in Energy Storage Power Station", *IAENG International Journal of Computer Science*, vol. 44, no. 4, pp. 471-481, 2017.

[2] K. W. E. Cheng, B. P. Divakar, and H. Wu, "Battery-management System (BMS) and SOC Development for Electrical Vehicles", *IEEE Transactions on Vehicular Technology*, vol. 60, no. 1, pp. 76-88, 2010.

[3] R. R. Kumar, C. Bharatiraja, and K. Udhayakumar, "Advances in Batteries, Battery Modeling, Battery Management System, Battery Thermal Management, SOC, SOH, and Charge/Discharge Characteristics in EV Applications", *IEEE Access*, vol. 11, pp. 105761-105809, 2023.

[4] J. P. Rivera-Barrera, N. Muñoz-Galeano, and H. O. Sarmiento-Maldonado, "SoC Estimation for LIBs: Review and Future Challenges", *Electronics*, vol. 6, no. 4, pp. 102, 2017.

[5] A. Clemente, A. Cecilia, and R. Costa-Castelló, "Online State of Charge Estimation for a Vanadium Redox Flow Battery with Unequal Flow Rates", *Journal of Energy Storage*, vol. 60, pp. 106503, 2023.

[6] L. Wang, X. Zhao, and Z. Deng, "Application of Electrochemical Impedance Spectroscopy in Battery Management System: State of Charge Estimation for Aging Batteries", *Journal of Energy Storage*, vol. 57, pp. 106275, 2023.

[7] C. Huang, H. Wu, and Z. Li, "Interacting Multiple Model for LIBs State of Charge Estimation Based on the Electrochemical Impedance Spectroscopy", *Electronics*, vol. 12, no. 4, pp. 808, 2023.

[8] Y. Gao, G. L. Plett, and G. Fan, "Enhanced State-of-charge Estimation of LiFePO4 Batteries Using an Augmented Physics-based Model", *Journal of Power Sources*, vol. 544, pp. 231889, 2022.

[9] L. Chen, W. Yu, and G. Cheng, "State-of-charge Estimation of Lithium-ion Batteries Based on Fractional-order Modeling and Adaptive Square-root Cubature Kalman Filter", *Energy*, vol. 271, pp. 127007, 2023.

[10] T. Gu, J. Sheng, and Q. Fan, "The Modified Multi-innovation Adaptive EKF Algorithm for Identifying Battery SOC", *Ionics*, vol. 28, no. 8, pp. 3877-3891, 2022.

[11] Q. Wang, M. Ye, and M. Wei, "Deep Convolutional Neural Network Based Closed-loop SOC Estimation for LIBs in Hierarchical Scenarios", *Energy*, vol. 263, pp. 125718, 2023.

[12] Z. Huang, Y. Zhou, and Z. Deng, "Precise State-of-Charge Mapping via Deep Learning on Ultrasonic Transmission Signals for LIBs", *ACS Applied Materials & Interfaces*, vol. 15, no. 6, pp. 8217-8223, 2023.

[13] H. Zhao, Z. Chen, and X. Shu, "State of Health Estimation for LIBs Based on Hybrid Attention and Deep Learning", *Reliability Engineering & System Safety*, vol. 232, pp. 109066, 2023.

[14] S. Huang. "Time Series Prediction Based on Improved Deep Learning", *IAENG International Journal of Computer Science* , vol. 49, no. 4, pp. 1133-1138, 2022.

[15] J. Chen, Y. Zhang, and J. Wu, "SOC Estimation for LIBs Using the LSTM-RNN with Extended Input and Constrained Output", *Energy*, vol. 262, pp. 125375, 2023.

[16] L. Xu, J. Wang, and Q. Chen, "Kalman Filtering State of Charge Estimation for Battery Management System Based on a Stochastic Fuzzy Neural Network Battery Model", Energy Conversion & Management, vol. 53, no. 1, pp. 33-39, 2012.